Preventing the Destruction of Aircraft Flap Cove Seals: An Aeroacoustic Fluid-Structure Interaction Benchmark Experiment

Christian Jente[1], Roland Ewert[2], Andreas Schröder[3], Tania Kirmse[3], Ramón Abarca[4]

1 Deutsches Zentrum für Luft- und Raumfahrt e.V., 38108 Braunschweig, Germany, email: christian.jente@dlr.de
2 Deutsches Zentrum für Luft- und Raumfahrt e.V., 38108 Braunschweig, Germany, email: roland.ewert@dlr.de
3 Deutsches Zentrum für Luft- und Raumfahrt e.V., 37073 Göttingen, Germany
4 Airbus Operations SL, 28906 Getafe/Madrid, Spain

Introduction

Flap cove seals must withstand fluid inertial forces while maintaining shape. This requires a multidisciplinary design integrating aerodynamics, fluid-structure interaction (FSI), and aeroacoustics.

The retraction of the flap from high-lift wing into cruise contour is particularly challenging at high speed. The final closing phase, especially at flap deflection angles of 2° to 3° can contain unwanted flow-seal interactions.

An experimental study was conducted in July 2025 at the Aeroacoustic Wind Tunnel Braunschweig (AWB) within the EU FALCON project. The seal was tested under nominal conditions, dynamically excited, and progressively loaded to near-failure. The seal, flap cove geometry, and deflection angles were adapted. Yet, the results capture key physical mechanisms relevant to full-scale operation.

A reduced dataset will be released as the Aeroacoustic FSI Test Case 2 (TC2) Benchmark problem. Data access is available upon request via DLR.

Test facility

AWB is a research facility for the Technical Acoustics department of the German Aerospace center (DLR), located in Braunschweig/Northern Germany.

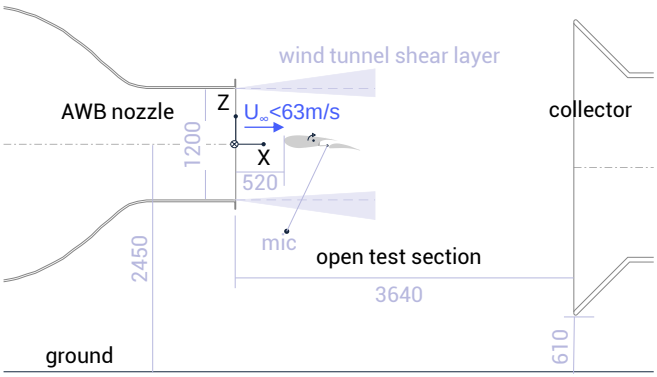

Figure 1: Open test section of the AWB wind tunnel test facility

The closed-circuit tunnel has an open test section with a 0.8 m x 1.2 m nozzle (width ΔY x height ΔZ, see figure 1). Flow velocities up to 63 m/s pass through a semi-anechoic measurement room (test section ΔX=3.64m) which is characterized by a lower cut-off frequency of about 200 Hz for broadband noise.
An adaptive collector can be adjusted to account for any flow deflections that are induced by high-lift wings.

Model wing with a large flap cove

The FALCON wing model (F15LSmod) uses the large flap-cove (scale ~1:3.67) from F15LS [1]. To adapt the large-scale model to AWB constraints, numerical simulations informed the test design, enabling an aerodynamically optimized short wing nose contour (new chord length: c = 700.8 mm), optimal installation position, wing incidence, and boundary layer fence configuration (see figures 2 and 3).

The flap cove was slightly modified to accommodate the seal holder (figure 2). The presented seal models are made of steel, required for compatibility with the PIV laser setup. Compared to the actual aircraft seal, the model is longer and thinner. The flap deflection angle was fixed at $\delta_F = 8°$.

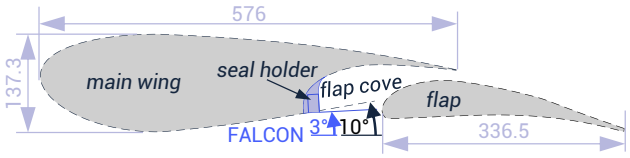

Figure 2: F15LSmod wing contour lines and adjustments in the flap cove for FALCON.

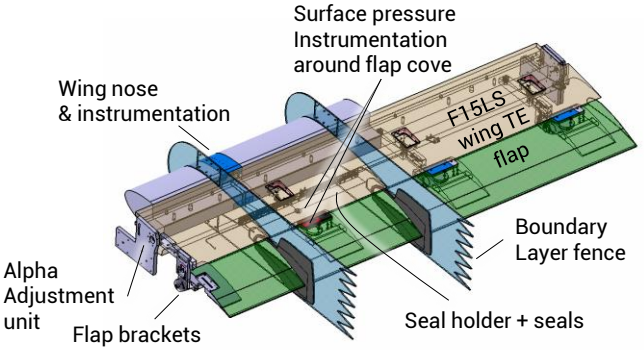

Figure 3: Parts of the F15LSmod 2 element wing

Instrumentation

The following instrumentation was installed to capture a comprehensive dataset:

- Pressure taps to validate wing aerodynamics,
- Microphones and surface pressure sensors for acoustic and pressure measurements,
- A surveillance camera for visual monitoring,
- Particle Image Velocimetry (PIV) to resolve the velocity field near the seal,
- Image Pattern Correlation Technique (ICPT) to track seal motion.

Tonal data analysis

The following analysis focuses only on the tonal data of the flush-mounted surface pressure sensors (figure 4) and the out-of-flow microphone installed under the wing (see figure 1).

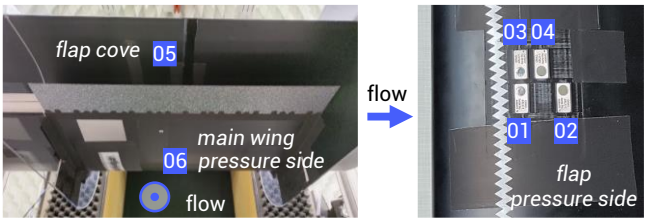

Figure 4: GRAS 48LX-1 UTP surface sensor positions

Tonal frequencies are extracted from the measured power spectral density (PSD) data at surface sensors 2 and 5 using a median filter-based approach.
The physical effects can be separated by plotting wind tunnel velocity vs. tonal frequencies (equation 1) in log-log spacing and determining the slope q of the resulting trend lines:

$$f \propto U^q, q = \begin{cases} 1 & \text{Vortex shedding} \\ 0.7 \dots 0.9 & \text{Rossiter} \\ 0 & \text{FSI tones/Bending} \end{cases} \quad (1)$$

Rossiter tones due to flow over an open cavity

Rossiter tones [2] are generated due to flow over an open cavity (figure 5). Turbulent vortices form at the seal trailing edge and convect downstream towards the wing trailing edge. Upon reaching the wing trailing edge, the vortices scatter into the free-field and propagate back to the seal trailing edge as acoustic waves. This completes the feedback loop.

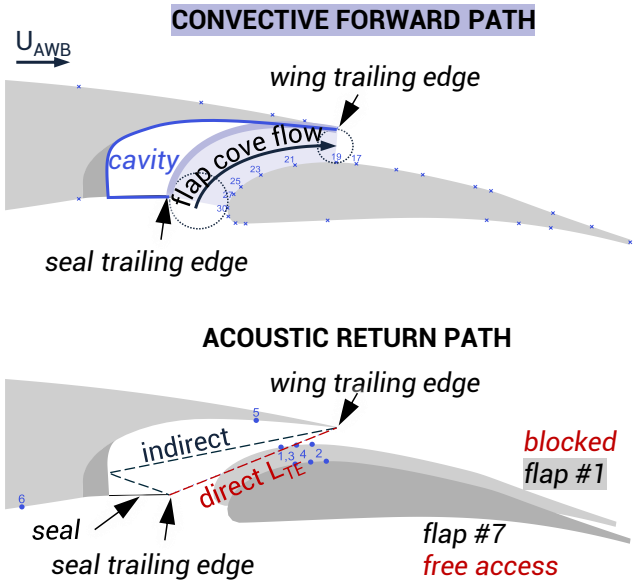

Figure 5: Feedback loop of the Rossiter effect which describes the tone generation caused by flow over an open cavity. Top: forward path, bottom: return path.

Figure 6 illustrates how the **accessibility of the direct acoustic return path** influences open cavity tones, by comparing top versus bottom sub-figures:

a) A configuration with an accessible direct acoustic return path can produce a propagating Rossiter effect, here the 2nd Rossiter mode, with high PSD. Beneath the base frequency, up to 2 harmonics are observed.

b) Blocking the direct return path with the flap significantly diminishes the tones and causes a weaker Rossiter effect (3rd Rossiter mode, reduced gain, no harmonics). This configuration achieves low-noise performance without inducing structural damage to the seal.

An aerodynamic effect emerges when the flap cove inlet area is smaller than the outlet area (AR_0<1). Under significant fluid inertial forces (C_B^*>2) the seal curves in order to improve the aerodynamic properties of the flap cove duct. The **curved seal** (right column) can be compared to the **straight seal** (left column):

c) The curved seal configuration can produce a propagating Rossiter effect with high gains and up to 2 harmonics to the base frequency. Compared to case a) there are shifts in the slope q and mode number (3rd Rossiter mode) which present a challenge for modelling.

d) Blocking the direct return path in the curved seal surpresses the Rossiter effect, offering acoustic benefits. However, this setup risks seal damage during flap closure. Therefore, this configuration must be avoided in practical applications.

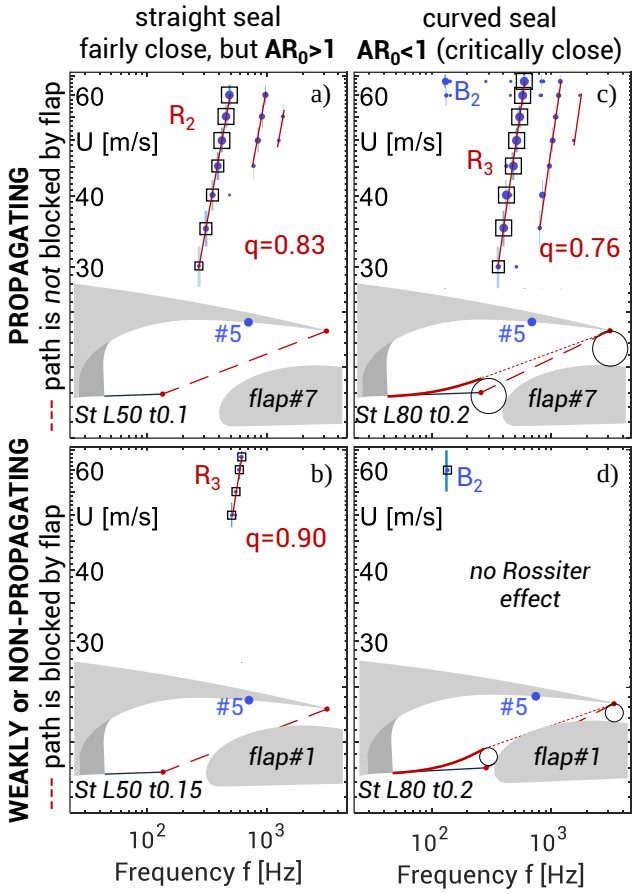

Figure 6: Rossiter effect depending on accessibility of the direct acoustic return path and shape of seal due to fluid loading. Tonal data from surface sensor #5 is displayed as contour plot (| vertical blue lines), ● dots are identified tones, □ squares represent the maximal gain for each test point. Flap position and seal length determine the duct's inlet to outlet area ratio AR_0.

Fluid-structure-interaction tones

The quasi-static seal shape (either straight or curved) and its dynamic excitation (see figure 8) are determined by the flap cove duct inlet-to-outlet area ratio AR_0 and the dimensionless bending compliance C_B^* (figure 7). The different seal states are illustrated in figure 11, based on the full test data.

The **flap cove duct inlet-to-outlet area ratio AR_0** (see figure 7 and equation 2) is analyzed in CAD under the assumption of a rigid seal at rest.

$$AR_0 = \frac{\text{Inlet}}{\text{Outlet}} = \frac{\Delta(\text{SealTE} - \text{FlapLE})}{\text{Gap}} \qquad (2)$$

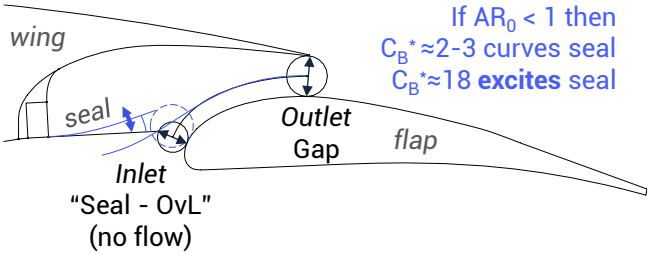

Figure 7: FSI seal excitation criterion

The **dimensionless bending compliance C_B^*** is defined (equations 3 and 4) as the ratio of fluid inertial force and bending stiffness. It is the inverse ratio of the commonly used dimensionless bending stiffness K_B^* [3]. Higher values of C_B^* correspond to greater seal tip deflections.

$$C_B^* := {K_B^*}^{-1} = \frac{\text{Fluid Inertial Force}}{\text{Plate bending Stiffness}} \propto \frac{\delta_{tip}}{L} \qquad (3)$$

$$C_B^* = \underbrace{\rho_\infty U_\infty^2}_{Aero} \underbrace{\frac{12(1-\nu^2)}{E}}_{Seal\ Material} \underbrace{\left(\frac{L}{t}\right)^3}_{Geom.} \qquad (4)$$

The fluid inertial force acting on the seal is approximated with the free-field properties of density ρ_∞=1.225 kg/m³ and U_∞ (local properties may be more precise). The material properties are Young's Modulus E=185 GPa and Poisson ratio ν=0.29 for Steel 1.4310. The seal geometry is defined by the aspect ratio between seal length L and thickness t.

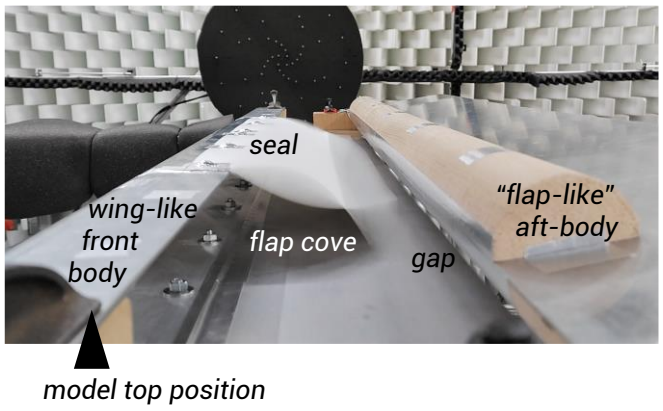

Figure 8: 2nd bending mode of the seal excited with high dynamic amplitude during FALCON AWB Pre-Test 2024

The test illustrated in figure 9 features progressively increasing flap cove inlet areas, achieved by changing the flap's overlap parameter.

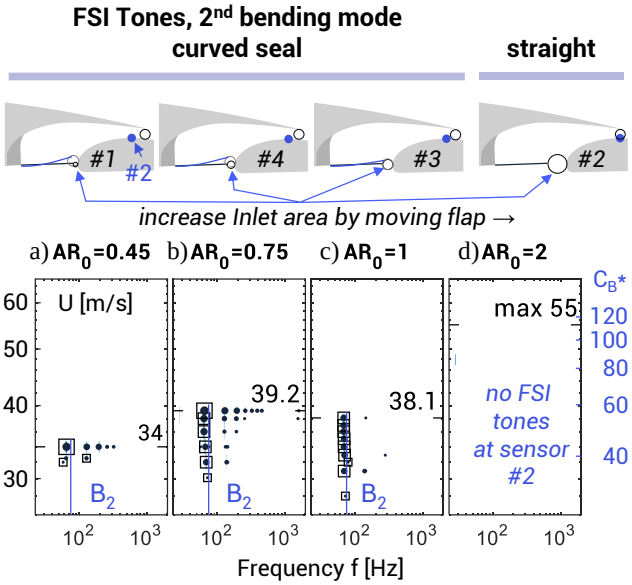

Figure 9: FSI-Tones depending on Area ratio AR_0 for different flap positions using the steel seal St L80 t0.1, evaluated at sensor #2.

Conventional flap cove flow is characterized by a converging duct geometry (AR_0>1) The seal is not particularly important in the consideration of pressure losses and flow discharge.

- At AR_0 = 2, (figure 9d), the seal remains straight and undeflected, enabling safe testing even at high wind tunnel velocities.
- At C_B^* = 100, the seal exhibits increasingly erratic, three-dimensional motion, with dominant deformation localized at the free corners and driven by longitudinal (spanwise) wave modes.
- The test was typically stopped when the sideways alu high speed tapes of the seal clamping mechanism were damaged to prevent further structural failure at C_B^* = 200 (figure 10).

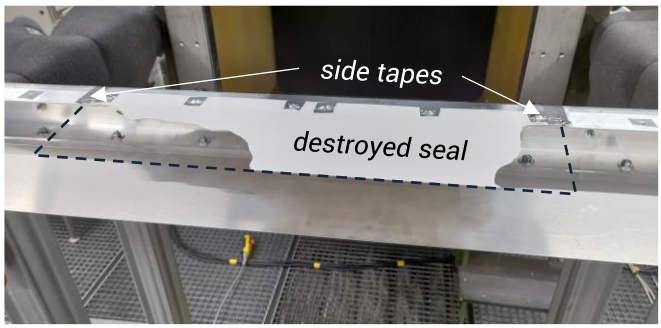

Figure 10: Polystyrene seal after a test run in December 2024.

At $AR_0 \leq 1$, a stiff seal restricts the flap cove flow due to its small inlet area, resulting in high flow turning losses. Compliant seals, such as the L80°t0.1 shown in figure 9a,b,c, adapt their shape to increase discharge and minimize pressure losses.

- At C_B^*=2…3, the characteristic quasi-static seal curving is observed. Even moderately low flow speeds can be sufficient to recreate the converging duct geometry

($AR(U_\infty)\geq 1$). Simultaneously, this increases stiffness against the longitudinal waves observed at $AR_0>1$. However, the curved seal is at risk of being squeezed and crushed during flap retraction.

- At $C_B^*=18$ the second bending mode of the seal is excited, but not acoustically audible. The seal exhibits small-amplitude vibrations around the quasi-static curved configuration, with no significant dynamic displacement.
- At $C_B^*\approx 50$, the out-of-flow mic detects the flow induced FSI tones. The number of higher harmonics causes the signal to be clearly audible to the experimenter. The seal deflection becomes significant (see figure 8).
- Higher ratios of C_B^* result in even higher amplitudes, leading to underdamping and accelerated material fatigue.

The undamped frequency of the second bending mode of a cantilever beam is given by equation 5:

$$f_2 = \frac{(4.6941)^2}{2\pi}\, t \sqrt{\frac{Eb}{12\rho L^3}} \qquad \text{[Hz]} \qquad (5)$$

where b is the spanwise width and ρ is the density of the seal.

Summary

Flap cove seal destruction can be prevented by maintaining the flap closer to the wing contour rather than to the seal ($AR_0>1$) during the flap retraction. Otherwise, moderately low velocities will curve the seal and risk its squeezing.

The Rossiter effect is strongly suppressed once the direct acoustic feedback is blocked.

Outlook: Benchmark test case data

The FALCON project releases an aero acoustic FSI benchmark test case (figures 11 and 12) to validate FSI modules in numerical codes, especially Lattice-Boltzmann solvers.

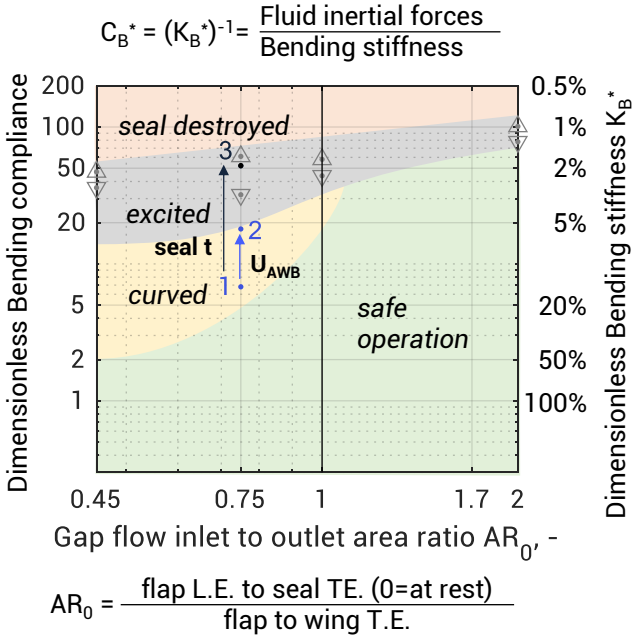

Figure 11: State of seal depending on dimensionless bending compliance and flap cove duct area ratio. Available benchmark datasets 1,2 and 3.

Benchmark data set 1 features the L80 t0.2 seal in a non-excited state with the wind tunnel operated at ~34.3m/s.

- Increasing the wind tunnel speed to 60m/s (1-2) triggers FSI tones (data set 2). The seal remains curved and at a very low dynamic motion.
- Reducing the trailing edge thickness (1-3) induces significant dynamic seal motion and excites FSI tones to up the 6th harmonic and beyond.

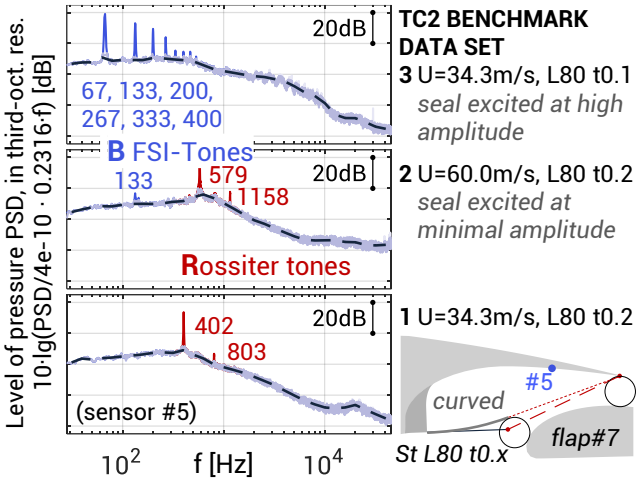

Figure 12: Spectral data of TC2 benchmark datasets 1,2 and 3 featuring different states of seal excitation and dynamic motion.

Acknowledgements

The authors gratefully acknowledge the contributions of all partners involved in the test design, manufacturing and conduction. Special thanks to the DLR test teams from Braunschweig and Göttingen, as well as to the Airbus partners for their invaluable support.

Funded by the European Union

Funded by the European Union's Horizon 2020 research and innovation programme under grant agreement No 101138305. Views and opinions expressed are however those of the author only and do not necessarily reflect those of the European Union or the European Commission. Neither the European Union nor the granting authority can be held responsible for them.

Literature

[1] Pott-Pollenske, M., Delfs, J., and Reichenberger, J., "A Testbed for Large Scale and High Reynolds Number Airframe Noise Research," 19th AIAA/CEAS, 2013. https://doi.org/10.2514/6.2013-2260

[2] Rossiter J.E.: Wind-tunnel experiments on the flow over rectangular cavities at subsonic and transonic speeds, Aeronaut. Res. Counc. Reports Memo., Technical Report 3438, 1964

[3] Duan F, Wang J.: Fluid–structure–sound interaction in noise reduction of a circular cylinder with flexible splitter plate. Journal of Fluid Mechanics. 2021;920:A6. https://doi.org/10.1017/jfm.2021.403